Journal of Hydroscience and Hydraulic Engineering
Vol. 22, No.2 November, 2004, 25-35

MUTUAL EFFECTS OF BED AND BANK DEFORMATION IN CHANNEL PLANE FORMATION

By

Yasuyuki Shimizu

Associate Professor, Graduate School of Engineering,
Hokkaido University, Sapporo, Japan

SYNOPSIS

A numerical model is proposed to simulate the formation of braided stream, in which bank erosion and bed deformation are calculated simultaneously. Flow field, bed deformation, bank erosion and channel geometry are calculated numerically by means of a general coordinate system, which can be applied to any shape of channel geometry during the channel evolution due to the bank erosion. Calculation is conducted with a initial narrow straight channel with flat bed, and in turn the development of alternate bar, channel meandering, appearance of mid channel bar, and finally, a braided channel geometry is simulated. Computational results are favorably compared with experiment. Interaction between the bank and bed deformation to the channel plane geometry is described.

INTRODUCTION

Determining the erosion of riverbeds and riverbanks quantitatively is an important area of research in disaster prevention works. The riverbed erosion in a fixed bank (experimental flumes, rivers with bank protection works, etc.) has been studied on theoretical and experimental basis and numerical models have been proposed. The mechanism of river bed forms has been examined, and numerical models are being established (e.g. Shimizu et al. (10)). Bank erosion and river meandering have been studied theoretically and experimentally, making it possible to understand these events to some extent(see e.g. Hasegawa & Ito (4), Parker (8)).

The changes in the bed topography and the erosion of banks are not events that occur independently; both of them take place interdependently through water flow and sediment. In order to evaluate such events, particularly for natural rivers, where banks are not protected, a model is required that can deal with riverbed evolution and bank erosion simultaneously. From this point of view, this study aims to develop such a model. The preliminary aim of this paper to describe a model for predicting river channels whose beds and banks consist of sandy soil. The basis of the model was the computation of a two-dimensional flow and the bed deformation. In order to make these computations, general coordinates, enabling a description of a boundary shape that takes an arbitrary form, is used assuming that erosion and sediment deposition occur along the channel boundary to transform the plane shape of the water channel into an arbitrary shape. Flow field is calculated using a high-order Godunov scheme referred to as the CIP method (Yabe & Ishikawa(11)). It is assumed that the erosion of banks occurs when the gradient in the cross-sectional direction of the banks is steeper than the submerged angle of repose, because of changes in the riverbed erosion near the banks. In this case, the amount of sediment beyond the submerged critical angle of slope is included in the computation of the bankbed evolution, as a supply of sediment from the banks. On the other hand, the inner banks at the channel bends and other parts, which are transformed into land, are successively excluded from the range of computation.

The computational model is verified by a physical model experiment conducted by Bertoldi *et al*(2). The experimental results show that the model is effective in simulating precisely the bank erosion and riverbed evolution, i.e. spatial and temporal changes of free meandering and bar formation. The model also proved that it is possible to quantitatively analyze the formation of multi-row bar channel or braided channel.

BASIC EQUATIONS OF FLOW

A moving boundary fitted coordinate (MBFC) system is employed for the flow and bed deformation in the domain where the channel width changes with time. Flow equations in cartesian coordinates are given as follows:

$$\frac{\partial h}{\partial t}+\frac{\partial (hu)}{\partial x}+\frac{\partial (hv)}{\partial y}=0 \tag{1}$$

$$\frac{\partial (hu)}{\partial t}+\frac{\partial (hu^2)}{\partial x}+\frac{\partial (huv)}{\partial y}=-gh\frac{\partial H}{\partial x}-C_d u\sqrt{u^2+v^2}+h\nu_t\left(\frac{\partial^2 u}{\partial x^2}+\frac{\partial^2 u}{\partial y^2}\right) \tag{2}$$

$$\frac{\partial (hv)}{\partial t}+\frac{\partial (huv)}{\partial x}+\frac{\partial (hv^2)}{\partial y}=-gh\frac{\partial H}{\partial y}-C_d v\sqrt{u^2+v^2}+h\nu_t\left(\frac{\partial^2 v}{\partial x^2}+\frac{\partial^2 v}{\partial y^2}\right) \tag{3}$$

where x and y are the cartesian coordinates, t is the time, u and v are the depth averaged velocity components in x- and y- directions, respectively, h is depth, H is the water surface elevation, g is the acceleration of gravity, and C_d is the bed friction coefficient.

The above equations are transformed into MBFC system in (ξ,η,τ) coordinates using the following relations:

$$\left\{\begin{array}{l}\dfrac{\partial}{\partial t}=\dfrac{\partial \tau}{\partial t}\dfrac{\partial}{\partial \tau}+\dfrac{\partial \xi}{\partial t}\dfrac{\partial}{\partial \xi}+\dfrac{\partial \eta}{\partial t}\dfrac{\partial}{\partial \eta}\\ \dfrac{\partial}{\partial x}=\dfrac{\partial \tau}{\partial x}\dfrac{\partial}{\partial \tau}+\dfrac{\partial \xi}{\partial x}\dfrac{\partial}{\partial \xi}+\dfrac{\partial \eta}{\partial x}\dfrac{\partial}{\partial \eta}\\ \dfrac{\partial}{\partial y}=\dfrac{\partial \tau}{\partial y}\dfrac{\partial}{\partial \tau}+\dfrac{\partial \xi}{\partial y}\dfrac{\partial}{\partial \xi}+\dfrac{\partial \eta}{\partial y}\dfrac{\partial}{\partial \eta}\end{array}\right. \tag{4}$$

or,

$$\left(\begin{array}{c}\dfrac{\partial}{\partial t}\\ \dfrac{\partial}{\partial x}\\ \dfrac{\partial}{\partial y}\end{array}\right)=\left(\begin{array}{ccc}\tau_t & \xi_t & \eta_t\\ \tau_x & \xi_x & \eta_x\\ \tau_y & \xi_y & \eta_y\end{array}\right)\left(\begin{array}{c}\dfrac{\partial}{\partial \tau}\\ \dfrac{\partial}{\partial \xi}\\ \dfrac{\partial}{\partial \eta}\end{array}\right) \tag{5}$$

where,

$$\tau_t=\frac{\partial \tau}{\partial t},\ \tau_x=\frac{\partial \tau}{\partial x},\ \tau_y=\frac{\partial \tau}{\partial y},\ \xi_t=\frac{\partial \xi}{\partial t},\ \xi_x=\frac{\partial \xi}{\partial x},$$

$$\xi_y=\frac{\partial \xi}{\partial y},\ \eta_t=\frac{\partial \eta}{\partial t},\ \eta_x=\frac{\partial \eta}{\partial x},\ \eta_y=\frac{\partial \eta}{\partial y} \tag{6}$$

Velocity components are transformed as follows:

$$u^\xi=\xi_x u+\xi_y v;\ \ u^\eta=\eta_x u+\eta_y v \tag{7}$$

or,

$$\left(\begin{array}{c}u^\xi\\ u^\eta\end{array}\right)=\left(\begin{array}{cc}\xi_x & \xi_y\\ \eta_x & \eta_y\end{array}\right)\left(\begin{array}{c}u\\ v\end{array}\right);\ \left(\begin{array}{c}u\\ v\end{array}\right)=\frac{1}{J}\left(\begin{array}{cc}\eta_y & -\xi_y\\ -\eta_x & \xi_x\end{array}\right)\left(\begin{array}{c}u^\xi\\ u^\eta\end{array}\right) \tag{8}$$

where u^ξ and u^η are contravariant components of flow velocity in the ξ- and η- directions. J is the Jacobian of the coordinate transformation, which can be written as follows:

$$J=\tau_t\xi_x\eta_y+\xi_t\eta_x\tau_y+\eta_t\tau_x\xi_y-\eta_t\xi_x\tau_y-\xi_t\tau_x\eta_y-\tau_t\xi_y\eta_x \tag{9}$$

Using these relations, the basic equations of flow in the MBFC system are given as follows:

$$\frac{\partial}{\partial \tau}\left(\frac{h}{J}\right)+\frac{\partial}{\partial \xi}\left[\left(\xi_t+u^\xi\right)\frac{h}{J}\right]+\frac{\partial}{\partial \eta}\left[\left(\eta_t+u^\eta\right)\frac{h}{J}\right]=0 \tag{10}$$

$$\frac{\partial u^\xi}{\partial \tau}+\left(\xi_t+u^\xi\right)\frac{\partial u^\xi}{\partial \xi}+\left(\eta_t+u^\eta\right)\frac{\partial u^\xi}{\partial \eta}+\alpha_1 u^\xi u^\xi+\alpha_2 u^\xi u^\eta+\alpha_3 u^\eta u^\eta-D_\xi$$

$$= -g\left[\left(\xi_x{}^2+\xi_y{}^2\right)\frac{\partial H}{\partial \xi}\left(\xi_x\eta_x+\xi_y\eta_y\right)\frac{\partial H}{\partial \eta}\right]-\frac{C_d u^\xi}{hJ}\sqrt{\left(\eta_y u^\xi-\xi_y u^\eta\right)^2+\left(-\eta_x u^\xi-\xi_x u^\eta\right)^2} \tag{11}$$

$$\frac{\partial u^\eta}{\partial \tau}+\left(\xi_t+u^\xi\right)\frac{\partial u^\eta}{\partial \xi}+\left(\eta_t+u^\eta\right)\frac{\partial u^\eta}{\partial \eta}+\alpha_4 u^\xi u^\xi+\alpha_5 u^\xi u^\eta+\alpha_6 u^\eta u^\eta-D_\eta$$

$$= -g\left[\left(\eta_x{}^2+\eta_y{}^2\right)\frac{\partial H}{\partial \eta}\left(\xi_x\eta_x+\xi_y\eta_y\right)\frac{\partial H}{\partial \xi}\right]-\frac{C_d u^\eta}{hJ}\sqrt{\left(\eta_y u^\xi-\xi_y u^\eta\right)^2+\left(-\eta_x u^\xi-\xi_x u^\eta\right)^2} \tag{12}$$

where ξ and η are spatial and $\tau(=t$ in the present model) is time coordinates in MBFC system. D_ξ and D_η are momentum diffusion terms in $\xi-$ and $\eta-$ directions, respectively, which are described in Shimizu & Itakura (9). Coeficients denoted by α_1 to α_6 are given as follows:

$$\alpha_1=\xi_x\frac{\partial^2 x}{\partial \xi^2}+\xi_y\frac{\partial^2 y}{\partial \xi^2};\quad \alpha_2=2\left(\xi_x\frac{\partial^2 x}{\partial \xi\partial \eta}+\xi_y\frac{\partial^2 y}{\partial \xi\partial \eta}\right);\quad \alpha_3=\xi_x\frac{\partial^2 x}{\partial \eta^2}+\xi_y\frac{\partial^2 y}{\partial \eta^2} \tag{13}$$

$$\alpha_4=\eta_x\frac{\partial^2 x}{\partial \xi^2}+\eta_y\frac{\partial^2 y}{\partial \xi^2};\quad \alpha_5=2\left(\eta_x\frac{\partial^2 x}{\partial \xi\partial \eta}+\eta_y\frac{\partial^2 y}{\partial \xi\partial \eta}\right);\quad \alpha_6=\eta_x\frac{\partial^2 x}{\partial \eta^2}+\eta_y\frac{\partial^2 y}{\partial \eta^2} \tag{14}$$

SEDIMENT TRANSPORT EQUATIONS

The continuity equation of two-dimensional bedload transport in MBFC is represented by the following equation:

$$\frac{\partial}{\partial t}\left(\frac{z_b}{J}\right)+\frac{1}{1-\lambda}\left[\frac{\partial}{\partial \xi}\left(\frac{q^\xi}{J}\right)+\frac{\partial}{\partial \eta}\left(\frac{q^\eta}{J}\right)\right]=0 \tag{15}$$

where z_b is bed elevation, λ is porosity of bed material, and q^ξ and q^η are the contravariant components of the bedload transport rate per unit width in the ξ- and η- directions, which are expressed by assigning s to the direction of the streamline and n to the direction perpendicular to the streamline:

$$q^\xi=\frac{\partial \xi}{\partial s}q^s+\frac{\partial \xi}{\partial n}q^n=\left(\xi_x\frac{\partial x}{\partial s}+\xi_y\frac{\partial y}{\partial s}\right)q^s+\left(\xi_x\frac{\partial x}{\partial n}+\xi_y\frac{\partial y}{\partial n}\right)q^n \tag{16}$$

$$q^\eta=\frac{\partial \eta}{\partial s}q^s+\frac{\partial \eta}{\partial n}q^n=\left(\eta_x\frac{\partial x}{\partial s}+\eta_y\frac{\partial y}{\partial s}\right)q^s+\left(\eta_x\frac{\partial x}{\partial n}+\eta_y\frac{\partial y}{\partial n}\right)q^n \tag{17}$$

where q^s and q^n are the bedload transport rate components in $s-$ and $n-$directions, respectively. The following equation proposed by Hasgawa (6) is employed for the calculation of q^s.

$$q^s=\frac{17}{\cos\theta_b}\tau_*^{3/2}\left(1-\frac{\tau_{*c}}{\tau_*}\right)\left[1-\sqrt{\frac{2\tau_{*c}\cos\theta_b}{\tau_*}}+2\left(\tan\theta_b-\frac{\partial z_b}{\partial s}\right)\right]\sqrt{\left(\frac{\rho_s-\rho}{\rho}\right)gd^3} \tag{18}$$

where θ_b represents the channel reference slope in downstream direction, ρ_s is density of bed material, d is grain size of bed material, τ_* is non-dimensional bed shear stress, and τ_{*c} is critical non-dimensional bed shear stress obtained by using Iwagaki's equation. Equation 18 is based on Ashida & Michiue's (1) formula and was modified to take into account the gravitational effect as proposed by Kovacs & Parker(7).

q^n is given by the following formula proposed by Hasegawa (5).

$$q^n=q^s\left(\frac{h}{r_s}N_*-\sqrt{\frac{\tau_{*c}}{\mu_s\mu_k\tau_*}}\frac{\partial z_b}{\partial n}\right) \tag{19}$$

where r_s is the radius of curvature of a streamline, N_* is the coefficient of strength of secondary flow, μ_s is the static friction coefficient of sand grain, μ_k is the kinetic friction coefficient of sand grain. In the analysis, a constant of $N_*=$ 7.0 given by Engelund (3) is used, while μ_s and μ_k are set to 1.0 and 0.45, considering the properties of sand.

The first term on the right hand side of Equation 19 represents the intensity of secondary flow in response to the curvature of the stream line. The curvature of stream line is determined by the angle between the stream line ($s-$direction) and x-axis.

$$\frac{1}{r_s}=\frac{\partial \theta_s}{\partial s}=\frac{\partial}{\partial s}\left[\tan^{-1}\left(\frac{v}{u}\right)\right]=\frac{\partial}{\partial T}\left[\tan^{-1}(T)\right]\frac{\partial T}{\partial s}=\frac{1}{1+T^2}\frac{\partial T}{\partial s} \tag{20}$$

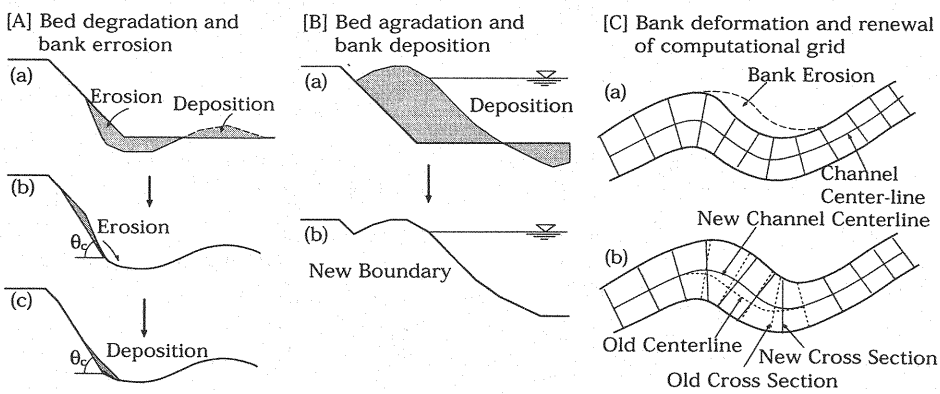

Figure 1: Bed deformation and renewal of channel geometry

where θ_s is the angle between $x-$ and $s-$axis, $T = v/u$, and,

$$\frac{1}{1+T^2} = \frac{1}{1+\left(\frac{v}{u}\right)^2} = \frac{u^2}{u^2+v^2} = \frac{u^2}{V^2} \tag{21}$$

$$\frac{\partial T}{\partial s} = \frac{\partial}{\partial s}\left(\frac{v}{u}\right) = \frac{u\dfrac{\partial v}{\partial s} - v\dfrac{\partial u}{\partial s}}{u^2} \tag{22}$$

$$\frac{\partial}{\partial s} = \frac{\partial x}{\partial s}\frac{\partial}{\partial x} + \frac{\partial y}{\partial s}\frac{\partial}{\partial y} = \frac{u}{V}\frac{\partial}{\partial x} + \frac{v}{V}\frac{\partial}{\partial y} = \frac{u}{V}\left(\xi_x\frac{\partial}{\partial \xi} + \eta_x\frac{\partial}{\partial \eta}\right) + \frac{v}{V}\left(\xi_y\frac{\partial}{\partial \xi} + \eta_y\frac{\partial}{\partial \eta}\right) \tag{23}$$

where $V = \sqrt{u^2+v^2}$. Consequently, r_s is determined by the following equation.

$$\frac{1}{r_s} = \frac{1}{V^3}\left[u^2\left(\xi_x\frac{\partial v}{\partial \xi} + \eta_x\frac{\partial v}{\partial \eta}\right) + uv\left(\xi_y\frac{\partial v}{\partial \xi} + \eta_y\frac{\partial v}{\partial \eta}\right)\right.$$
$$\left. -uv\left(\xi_x\frac{\partial u}{\partial \xi} + \eta_x\frac{\partial u}{\partial \eta}\right) - v^2\left(\xi_y\frac{\partial u}{\partial \xi} + \eta_y\frac{\partial u}{\partial \eta}\right)\right] \tag{24}$$

The channel bed slope in $s-$ and $n-$directions, $\partial z_b/\partial s$ and $\partial z_b/\partial n$ used in Eqs. 18 and 19, respectively, are expressed as follows:

$$\frac{\partial z_b}{\partial s} = \frac{\partial z_b}{\partial \xi}\frac{\partial \xi}{\partial s} + \frac{\partial z_b}{\partial \eta}\frac{\partial \eta}{\partial s} = \frac{\partial z_b}{\partial \xi}\left(\xi_x\frac{\partial x}{\partial s} + \xi_y\frac{\partial y}{\partial s}\right) + \frac{\partial z_b}{\partial \eta}\left(\eta_x\frac{\partial x}{\partial s} + \eta_y\frac{\partial y}{\partial s}\right) \tag{25}$$

$$\frac{\partial z_b}{\partial n} = \frac{\partial z_b}{\partial \xi}\frac{\partial \xi}{\partial n} + \frac{\partial z_b}{\partial \eta}\frac{\partial \eta}{\partial n} = \frac{\partial z_b}{\partial \xi}\left(\xi_x\frac{\partial x}{\partial n} + \xi_y\frac{\partial y}{\partial n}\right) + \frac{\partial z_b}{\partial \eta}\left(\eta_x\frac{\partial x}{\partial n} + \eta_y\frac{\partial y}{\partial n}\right) \tag{26}$$

Non-dimensional bed shear stress, τ_*, in Equations 18 and 19 is given by:

$$\tau_* = \frac{C_d V^2}{\left(\dfrac{\rho_s}{\rho-1}\right)gd} = \frac{C_d(u^2+v^2)}{\left(\dfrac{\rho_s}{\rho-1}\right)gd} \tag{27}$$

$\partial x/\partial s$, $\partial x/\partial n$, $\partial y/\partial s$ and $\partial y/\partial n$ in Equations (16), (17), (18) and (19) are given by:

$$\frac{\partial x}{\partial s} = \frac{u}{V} = \cos\theta_s;\quad \frac{\partial y}{\partial s} = \frac{v}{V} = \sin\theta_s;\quad \frac{\partial x}{\partial n} = -\frac{v}{V} = -\sin\theta_s;\quad \frac{\partial y}{\partial n} = \frac{u}{V} = \cos\theta_s \tag{28}$$

BANK EROSION AND CHANNEL MIGRATION

A ξ-axis is drawn along the channel for the given initial plane shape of the channel, and a η-axis is drawn to intersect with the ξ-axis. Then the plane (ξ, η) is properly divided into the parts to make the initial grids for the computations. The computations for the flow and the bed evolution are conducted using the equations described in the previous two sections. Focus is placed on the bed evolutions near the banks, and the deformations in the plane shape of the channel are calculated according to the following procedure: When computations show that the riverbed near the banks decreases in height and the cross-sectional gradient of the bank slope also becomes steeper than the submerged angle of repose (θ_c), the sediment beyond the submerged angle of repose is assumed to be momentarily eroded to the point of this submerged angle of repose [Hasegawa (5)]. Furthermore, it is assumed that the sediment load equal to the amount of sediment beyond submerged angle of repose, is deposited at the foot of the bank slope (Fig. 1[A]). At this time, if the erosion of the bank slope face advances toward the top of the slope, the computational range is enlarged in the cross-sectional direction of the channel. Moreover, if part of the bed near the banks is transformed into land, which causes a narrowing the water channel, the computational range is moved to the new waterline (Fig. 1[B]). When the computational range becomes enlarged, for example, due to the erosion of the banks (Fig. 1[C](a)), (Fig. 1[C](b)), (1) a new central line of the channel passing through the center of new banklines is set. (2) Along this new central line of the channel, new cross-sections perpendicular to this line are set at equal intervals as the initial condition in the η- direction. (3) Each cross-section is divided into the grid numbers in the ξ-direction. Thus, new computational meshes are formed, and the computational data are all transformed from old to new computational grid. While transforming all the computational data between the new and old grid, a linear transformation based on geometric locations must be carried out. These calculations are conducted at intervals of a infinitesimal time (Δt) and are continued up to the designated time. Note that the values of ξ_t and η_t are calculated through these processes and fed back into Equations 10, 11 and 12.

NUMERICAL MODEL

Equations of (10), (11) and (12) are solved numerically using the finite difference method with computational grids in (ξ, η) coordinate system. For Equations (11) and (12), a high-order Godunov scheme known as the Cubic Interpolated Psuedo-particle (CIP) method, proposed by Yabe & Ishikawa (11), is employed. The assumption is made that at very small time increments, the temporal change of the velocity components at a point in space can be broken down into the time evolution of the inhomogeneous terms and the time evolution at a point due to the advection of the field. Therefore, in the first step the change in time of the velocity (u^ξ and u^η denoted here as f) is solved as:

$$\frac{\partial f^*}{\partial t} = G \tag{29}$$

where G is the summation of non-advection terms in Equations (11) and (12), and $*$ denotes the values of non-advection phase. Then f is solved in the advection phase as

$$\frac{\partial f}{\partial \tau} + \tilde{u}\frac{\partial f}{\partial \xi} + \tilde{v}\frac{\partial f}{\partial \eta} = 0 \tag{30}$$

where $\tilde{u} = \xi_t + u^\xi$ and $\tilde{v} = \eta_t + u^\eta$. The solution of Equation (30) for small $\Delta\tau$ is simply approximated as:

$$f(\xi, \eta, \tau + \Delta\tau) \approx f(\xi - \tilde{u}\Delta\tau, \eta - \tilde{v}\Delta\tau, \tau) \tag{31}$$

Using the solution of the non-advection phase (Equation 29) this approximation becomes

$$f(\xi, \eta, \tau + \Delta\tau) \approx f^*(\xi - \tilde{u}\Delta\tau, \eta - \tilde{v}\Delta\tau, \tau + \Delta\tau) \tag{32}$$

The difficulty then is how to find the value of f^* at points in space which generally do not lie on the numerical grid points, as specified by the right hand side of Equation 32. If linear interpolation is used to find f^* at points not on the grid, the first order Godunov method is attained. A more accurate solution requires higher order interpolation, and thus high-order Godunov schemes. In the CIP method, a cubic interpolation of f^* is proposed, and when the interpolation is combined with Equation 32 the resultant equation for f at grid point i, j and time $n + 1$ is given by:

$$\begin{aligned} f_{i,j}^{n+1} = &\left[(a_1 X + c_1 Y + e_1)X + g_1 Y + f_\xi^*(i,j)\right] X + \\ &\left[(b_1 Y + d_1 X + f_1)Y + f_\eta^*(i,j)\right] Y + f^*(i,j) \end{aligned} \tag{33}$$

in which,

$$X = -\tilde{u}\Delta\tau; \quad Y = -\tilde{v}\Delta\tau; \quad f_\xi^* = \frac{\partial f^*}{\partial \xi}; \quad f_\eta^* = \frac{\partial f^*}{\partial \eta} \tag{34}$$

Table 1: Experimental condition of RUN B1.5-20 by Bertoldi *et al.*

Grain Size	d	1.3mm
Slope	S	1.5%
Water Discharge	Q	0.333×10^{-3} m^3/s
Sediment Discharge	Q_s	0.583 g/s

$$a_1 = \left\{\left[f_\xi^*(i+1,j) + f_\xi^*(i,j)\right]\Delta\xi + 2\left[f^*(i,j) - f^*(i+1,j)\right]\right\} / \left(\Delta\xi^3\right) \tag{35}$$

$$b_1 = \left\{\left[f_y^*(i,j+1) + f_y^*(i,j)\right]\Delta\eta + 2\left[f^*(i,j) - f^*(i,j+1)\right]\right\} / \left(\Delta\eta^3\right) \tag{36}$$

$$c_1 = \{f^*(i,j) - f^*(i,j+1) - f^*(i+1,j) + f^*(i+1,j+1) - \left[f_\xi^*(i,j+1) - f_\xi^*(i,j)\right]\Delta\xi\} / \left(\Delta\xi^2\Delta\eta\right) \tag{37}$$

$$d_1 = \{f^*(i,j) - f^*(i,j+1) - f^*(i+1,j) + f^*(i+1,j+1) - \left[f_\eta^*(i+1,j) - f_\eta^*(i,j)\right]\Delta\eta\} / \left(\Delta\xi\Delta\eta^2\right) \tag{38}$$

$$e_1 = \left\{3\left[f^*(i+1,j) - f^*(i,j)\right] - \left[f_\xi^*(i+1,j) + 2f_\xi^*(i,j)\right]\Delta\xi\right\} / \Delta\xi^2 \tag{39}$$

$$f_1 = \left\{3\left[f^*(i,j+1) - f^*(i,j)\right] - \left[f_\eta^*(i,j+1) + 2f_\eta^*(i,j)\right]\Delta\eta\right\} / \Delta\eta^2 \tag{40}$$

$$g_1 = \left[-f_\eta^*(i+1,j) + f_\eta^*(i,j) - c_1\Delta\xi^2\right] / \Delta\xi \tag{41}$$

In the above instance, it is assumed that $\widetilde{u}$ and $\widetilde{v}$ are negative, so that the advection to the grid points i, j is from within the area, whose vertices are (i,j), $(i+1,j)$, $(i,j+1)$ and $(i+1,j+1)$. When $\widetilde{u} \geq 0$ the index $i+1$ in Equations 35-41 should be changed to $i-1$, and in tern $\Delta\xi$ becomes $-\Delta\xi$. Similarly, when $\widetilde{v} \geq 0$, $j+1$ and $\Delta\eta$ becomes $j-1$ and $-\Delta\eta$. In the non-advection phase, f^* is calculated from the continuity equation by taking the divergence of the momentum equations and solving for depth as a Poisson equation. The viscous terms are approximated by means of central differences. Each velocity component is defined in the center of two faces of the computational cells, and depth is defined at the center of the cell. The general procedure, then, is to calculate f^* from Equation 29 in which the convective acceleration terms do not appear. In the second phase f is calculated at the grid points from a pure advection of the cubic interpolated field of f^* by Equations 33-41. These two steps complete the calculation of a single time increment, $\Delta\tau$. The CIP method makes it possible to solve the problem of boundedness while introducing little numerical diffusion and, further more, algorithm implementation is less complicated than other high-order upwind schemes.

APPLICATION OF THE MODEL

The proposed model is tested by an experiment conducted by Bertoldi *et al.* (2). The experiment was started with a straight trapezoidal cross section; its base was 0.06m wide and the bank slope was about 40°. During the experiment the evolution of the channel width was continuously monitored by taking pictures along the flume. Bottom topography was surveyed three times of 70, 130 and 150 minutes. Experimental conditions of RUN B1.5-20 are summarized in Table 1.

Calculations were conducted under the same conditions as the Bertoldi *et al's* experiment. Figure 2 shows the changes in the bed and the depth averaged flow velocity with time in the contour map. It is shown that the channel meandering proceeded while bank erosion took place which advanced on the right and left bank alternately. From the calculated results, sections A-A and B-B at 160 minutes are shown as examples of wide and narrow sections, respectively, in Figs. 3 and 4. Fig. 3 shows that a mid-channel bar was developed and the channel bifurcation or braiding was observed. Fig. 5 shows comparisons between observed and calculated results on the channel geometry and bed elevation at 70, 110 and 150 minutes. The time change of the general geometric characteristics was well reproduced by the prsented model.

EFFECT OF BANK STRENGTH IN CHANNEL PLANE GEOMETRY

In the present model, the strength of the bank against the lateral erosion is represented by the angle of repose, θ_c. The effect of the angle of repose to the morphological behavior of the bar and channel geometry are tested in this section. Fig. 6 shows the computational results with different values of θ_c. The large value of θ_c indicates the stronger bank, while the small value of θ_c represents the weaker bank such as sandy bank. Note that the angle of repose used here is not in a physical based meaning, but a parameter expresses the erosion-proof intensity

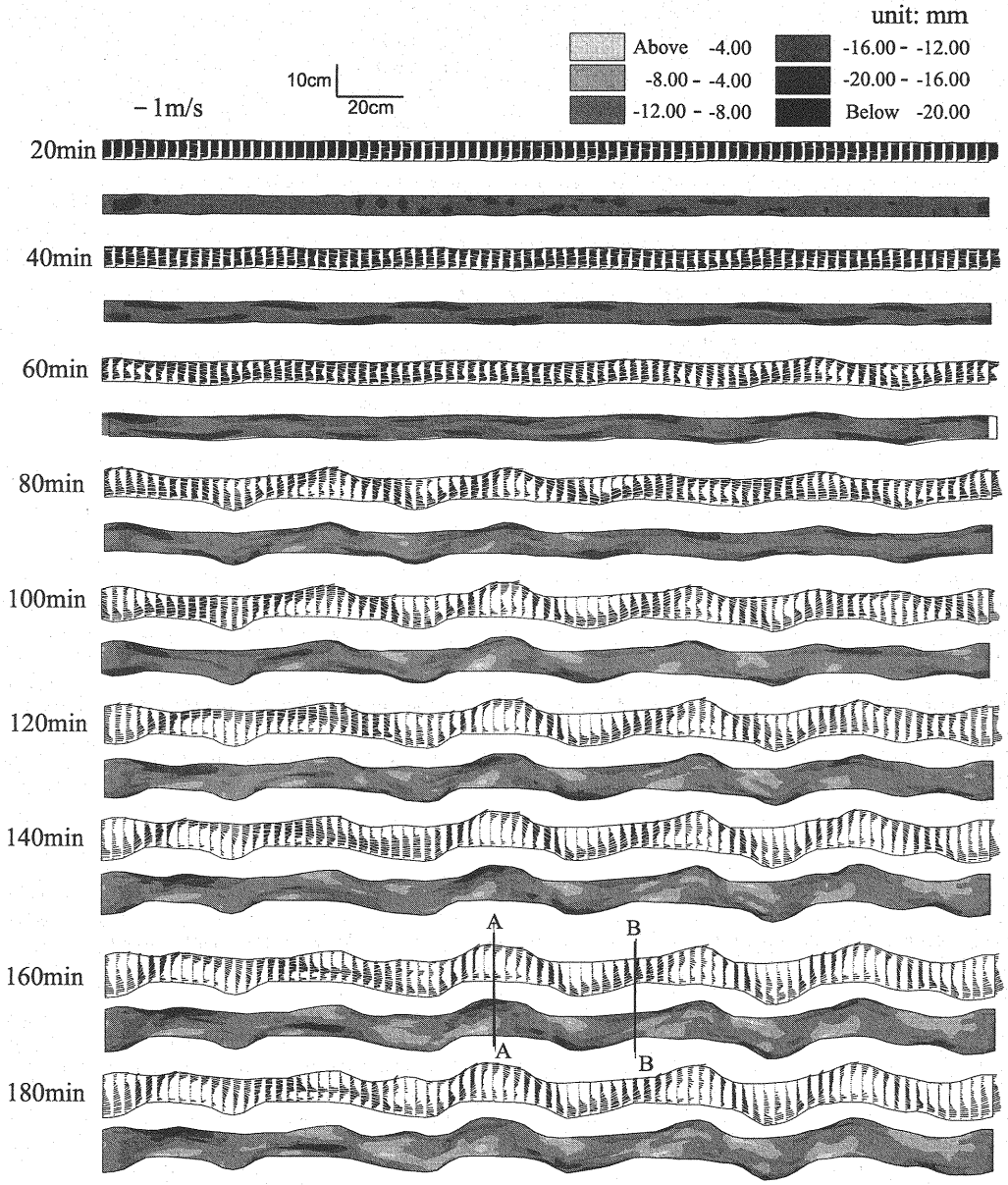

Figure 2: Calculated velocity vector, bed elevation and channel geometry

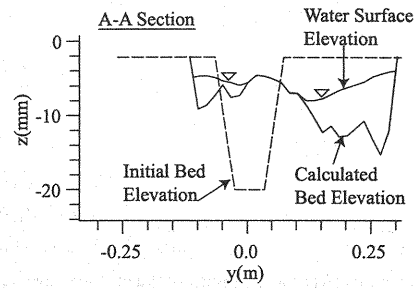

Figure 3: Calculated bed and water surface elevation of section A-A

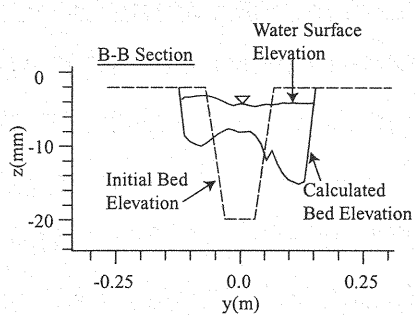

Figure 4: Calculated bed and water surface elevation of section B-B

for convenience. Fig. 6 shows that when θ_c is large, the channel dose not meander, but as θ_c becomes small the wavelength and the amplitude of channel plane geometry becomes large. This means that the formation of channel geometry depends considerably on the strength of bank material. For example, starting with no-bar condition at the initial state, the development of alternate bar causes the channel width expansion, and when the migration of the bar is trapped by the bends generated by the bank erosion, the places of the bed erosion are fixed and it amplifies the width expansion. Figure 7 shows the cross sections of Fig.6 at x=381cm with θ_c=0.6,1.0 and 1.5. When the angle of repose increases, the expansion of the channel tends to be suppressed. In contrast to this, channel width expansion rate becomes large with decreacing of θ_c and a mid-channel bar formed in this case.

CONCLUSION

As a first step fowards developing a numerical computation model to simulate the evolution of braided stream with bank erosion, a model which can calculate riverbed and riverbanks deformation simultaneously was proposed. A coordinate system was used for the computation in which the boundary can take arbitrary forms. The reason for this was that we assumed that erosion and sediment deposition occur laterally, thereby transforming the shape of a channel into arbitrary shapes. The erosion of banks was assumed to occur when the gradient in the cross-sectional direction of the bank becomes steeper than a submerged angle of repose, due to the changes in bed topography near the banks. In this case, the amount of sediment beyond the submerged angle of repose was included in the computation of the riverbed evolution as a supply of sediment from the banks. The model was verified by an experiment on channel widening and braided bar development. As a result, the model proved to be effective in simulating the changes in braiding accompanying bank erosion. This study provides evidence that the model can analyze the braided stream with bank erosion in sandy channel. Finally, the effect of bank strength in channel plane formation is tested by the proposed numerical model. It was found that the bank strength plays an important role in the formation of channel geometry.

REFERENCES

1. Ashida, K. and Michiue, M.: Study on hydraulic resistance and bed-load transport rate in alluvial streams. *Proc. of JSCE*, No.201, pp.59–69, 1972(in Japanese).

2. Bertoldi, W., Tubino, M. and Zolezzi, G.: Laboratory measurements on channel bifurcation. *Proc. of 2nd IAHR Symposium on River Coastal and Estuarine Morphodynamics*, pp.723–732, 2001.

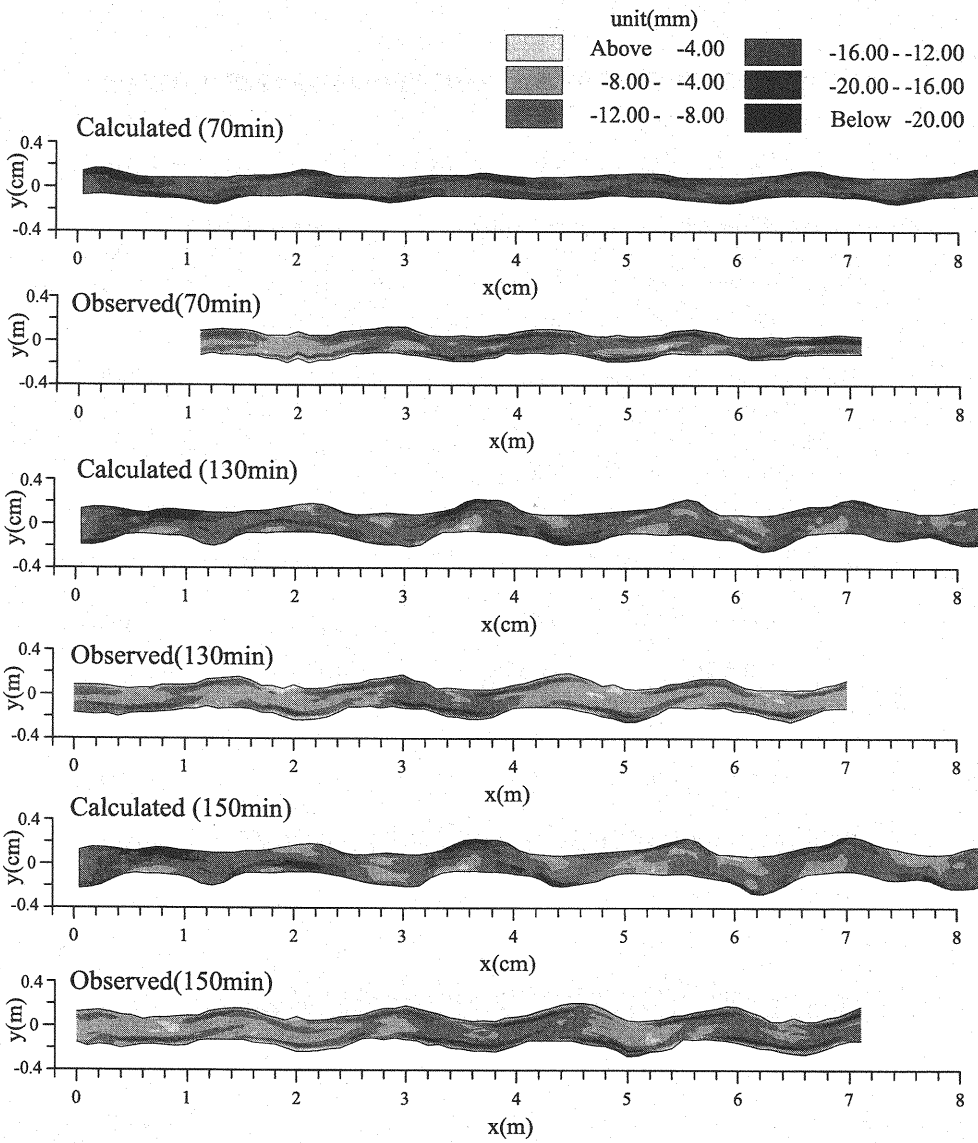

Figure 5: Comparison of bed elevation and channel geometry between calculated and experiment

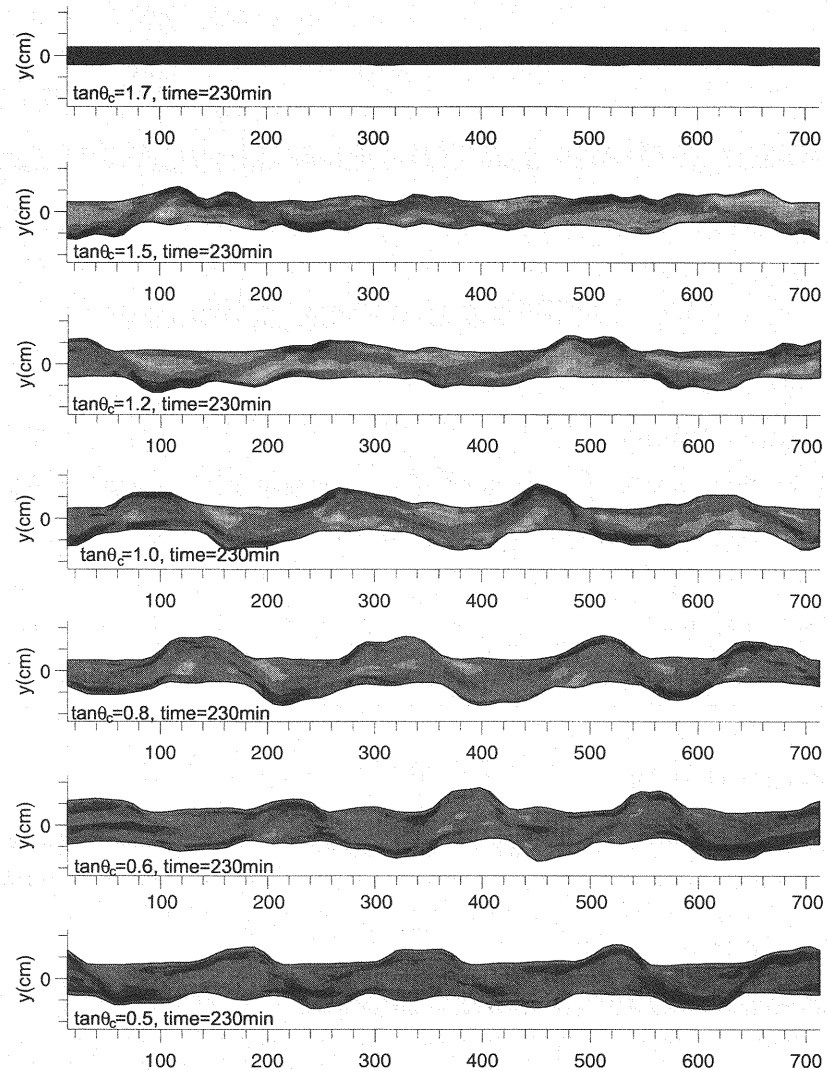

Figure 6: Comparison of channel geometries depends on erosion-proof strength of bank

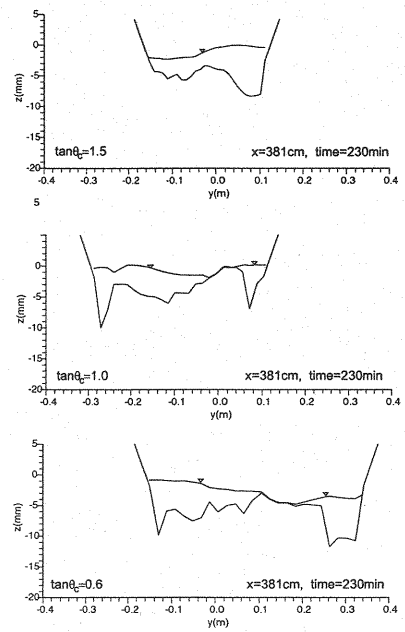

Figure 7: Comparison of channel cross sections depends on erosion-proof strength of bank

3. Engelund, F.: Flow and bed topography in channel bends. *J. Hyd. Div., ASCE*, 100(11), pp.1631–1648, 1974.

4. Hasegawa, K., and Ito, H. 1978. Computer simulation of the changing process by year in meandering channel. *Proc. of Hokkaido Chapter of JSCE*, No.32, pp.197–202, 1878(in Japanese).

5. Hasegawa, K.: Hydraulic research on planimetric forms, bed topographies and flow in alluvial rivers. *Ph. D. Dissertation, Hokkaido Univ., Japan*, 1–184, 1984(in Japanese).

6. Hasegawa, K.: Hydraulic Characteristics of montain streams and their practical application, *Lecture notes of the 33rd Summer Seminar on Hydrau. Engrg., JSCE*, A-9-1–20, 2001(in Japanese).

7. Kovacs, A. and Parker, G.: A new vectorial bedload formulation and its application to the time evolution of straight river channels. *Jour. of Fluid Mrch.*, 267, pp.153–183, 1994.

8. Parker, G. 1983. Theory of meander bend deformation, river meandering. *Proc. of Conf. Rivers'83, ASCE*, 1983.

9. Shimizu, Y. and Itakura, T. 1991. Calculation of flow and bed deformation with a general non-orthogonal coordinate system, *Proc. of XXIV IAHR Cong. Madrid, Spain*, Vol. C, pp.241-248, 1991.

10. Shimizu, Y., Watanabe, Y. and Toyabe, T. 1995. Finite amplitude bed topography in straight and meandering rivers. *J. Hyd. Coast. and Envir. Engrg., JSCE*, No.509, pp.67–78, 1995.

11. Yabe, T. and Ishikawa, T.: A numerical cubic-interpolated pseudoparticle (CIP) method without time splitting technique for hyperbolic equations, *Jour. of PSJ*, Vol.59, No.7, 2301–2304, 1990.

(Received July 7, 2003 ; revised March 30, 2004)